Multicolor Microcrystals

Deutsche Ausgabe: DOI: 10.1002/ange.201511626
Internationale Ausgabe: DOI: 10.1002/anie.201511626

Unraveling Epitaxial Habits in the $NaLnF_4$ System for Color Multiplexing at the Single-Particle Level

Yuhai Zhang, Ling Huang, and Xiaogang Liu**

Dedicated to Professor Wee Kiong Choi

Abstract: *We report an epitaxial growth technique for scalable production of hybrid sodium rare-earth fluoride ($NaLnF_4$) microcrystals, including $NaYF_4$, $NaYbF_4$, and $NaLuF_4$ material systems. The single crystalline nature of the as-synthesized products makes them strong upconversion emission. The freedom of combining a lanthanide activator (Er^{3+} or Tm^{3+}) with a sensitizer (Yb^{3+}) at various doping concentrations readily gives access to color multiplexing at the single-particle level. Our kinetic and thermodynamic investigations on the epitaxial growth of core–shell microcrystals using $NaLnF_4$ particle seeds suggest that within a certain size regime it is plausible to exert precise control over shell thickness and growth orientation under hydrothermal conditions.*

Crystal epitaxy is a research area of immense significance as the utility of this crystal-growth technique permits the fabrication of complex nanostructures, including core–shell semiconducting nanoparticles, segmented nanowires, sandwiched films, and hybrid nanoarrays.[1] In lanthanide-doped particle systems, the epitaxial growth technique not only offers fine control over the particle's emission intensity and colors,[2] but also provides an important tool to elucidate fundamental upconversion mechanisms.[3] However, phase separation and various strain-induced barriers may occur during epitaxial growth, thereby hindering the growth of particles beyond a certain volume and with a narrow size distribution.[2a,4] For example, a standard co-precipitation procedure for the epitaxial growth of core–shell upconversion nanoparticles usually results in a thin shell layer, typically less than 5 nm in thickness. To grow a much thicker layer, the same procedure has to be repeated multiple times while paying close attention to the increased possibility of phase separation. The main difficulty with this method is that the shell thickness is unlikely to reach 300 nm, a size regime typically required by the resolution of a conventional optical microscope for practical encoding and decoding purposes.[5] Apart from shell thickness, accurate control of growth orientation in epitaxial structures has also been challenging. Despite recent efforts,[6] there is no direct evidence supporting such an orientation preference during the epitaxial growth process. This partially stems from the fact that most electron microscopy techniques lack the ability to discern different types of lanthanide ions because of their similarity in size.

Our present attempts aim at developing an epitaxy approach to synthesizing core–shell upconversion microcrystals with well-defined shell thickness beyond 300 nm. Our approach is also able to provide fine control over epitaxial growth orientation along specific crystal facets. Importantly, we discover that the multiple colors emitted by these materials can be resolved at the single-particle level, making them ideal candidates as optical barcodes for multiplexed labeling and imaging applications.

The core–shell microcrystals were synthesized using modifications of methods based on hydrothermal conditions (Figure 1 a).[6b,7] In a typical experiment, $NaYF_4$:Yb/Er microcrystals were first prepared as seeds prior to epitaxial core–shell growth (Figure 1 b and Supporting Figures S1–S5). We next added a mixed solution containing NaF, H_2O, $LuCl_3$, $YbCl_3$, $TmCl_3$, and sodium citrate to the $NaYF_4$:Yb/Er microcrystals. Note that Yb^{3+}/Er^{3+} and Yb^{3+}/Tm^{3+} pairs are doped into the core and shell, respectively, to induce dual emission colors. Under optimal reaction conditions, the core–shell epitaxial growth occurs when the temperature reaches 220 °C. Transmission electron microscopy (TEM) imaging of the reaction product showed microcrystals with a lateral dimension of 4.4 μm on average, indicating the formation of an epitaxial shell of approximately 700 nm (Figure 1 c).

Figure 1 d shows an optical microscopic image of the $NaYF_4$:Yb/Er microcrystals on 980-nm laser excitation. The yellowish color arises from Er^{3+} emission. After core–shell epitaxial growth with added Tm^{3+} precursor, we observed distinct yellow and blue emission from the core and shell region of the resulting crystals (Figure 1 e). The synthesis produces high yields of monodispersed core–shell products, made evident by the observation of visible dual emission for almost all the samples under microscopic investigation.

[*] Y. Zhang, Prof. X. Liu
Department of Chemistry, National University of Singapore
3 Science Drive 3, Singapore 117543 (Singapore)
E-mail: chmlx@nus.edu.sg
Prof. X. Liu
Institute of Materials Research and Engineering, Agency for Science, Technology and Research
3 Research Link, Singapore 117602 (Singapore)
and
Center for Functional Materials, NUS (Suzhou) Research Institute
Suzhou, Jiangsu 215123 (China)
Prof. L. Huang
Key Laboratory of Flexible Electronics & Institute of Advanced Materials, Jiangsu National Synergistic Innovation Center for Advanced Materials, Nanjing Tech University
30 South Puzhu Road, Nanjing, 211816 (China)
E-mail: iamlhuang@njtech.edu.cn
Supporting information and the ORCID identification number(s) for the author(s) of this article can be found under http://dx.doi.org/10.1002/anie.201511626.

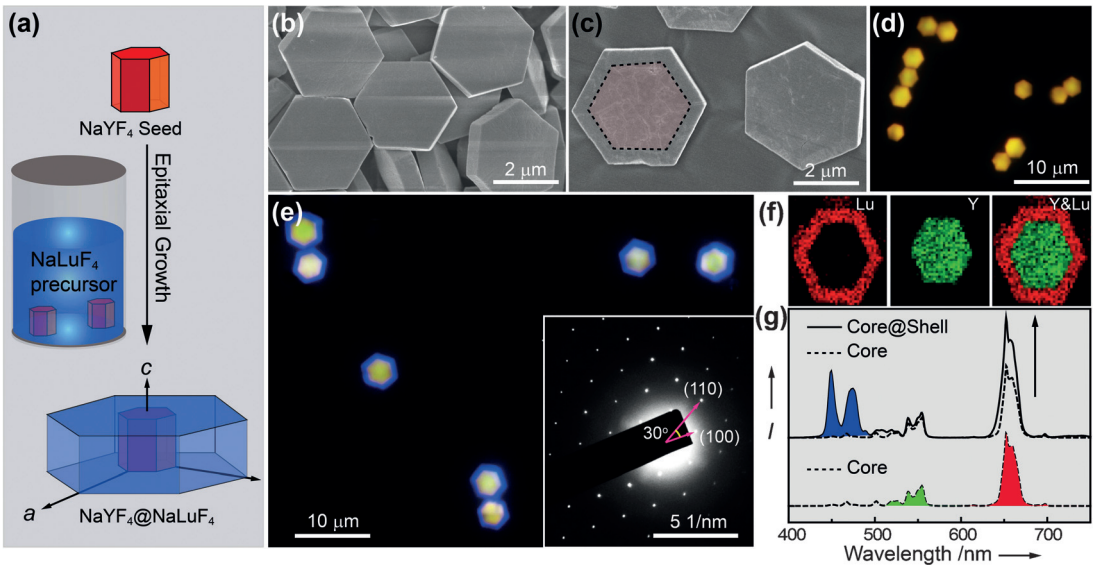

Figure 1. a) Schematic representation of the epitaxial growth process conducted in a hydrothermal reactor containing seeding crystals, $NaLuF_4$, and sodium citrate. b) Typical SEM image of hexagonal-phase $NaYF_4$:Yb/Er (20/0.5 mol%) seeding crystals. c) Corresponding SEM image of the as-synthesized $NaYF_4$:Yb/Er (20/0.5 mol%)@$NaLuF_4$:Yb/Tm (5/0.5 mol%) crystals after the epitaxial growth process. The pink hexagon with dotted lines in (c) marks the core component of the core–shell crystal. d,e) Upconversion luminescent micrographs of the core and core–shell crystals, respectively, on 980 nm laser excitation. The inset in (e) shows a selected area electron diffraction pattern taken at the edge of a core–shell crystal. f) Elemental mapping conducted on a single core–shell crystal by using an energy dispersive X-ray (EDX) spectrometer. g) Upconversion emission spectra of a single $NaYF_4$:Yb/Er (20/0.5 mol%)@$NaLuF_4$:Yb/Tm (5/0.5 mol%) microdisk (top) and the corresponding $NaYF_4$:Yb/Er (20/0.5 mol%) core particle (bottom). Blue indicates emission from Yb^{3+}/Tm^{3+} pair co-doped into the shell. Green and red indicate emission from the Yb^{3+}/Er^{3+} pair co-doped into the core.

Intriguingly, the characterization of the epitaxially grown shell by electron diffraction suggests its single-crystalline nature (Figure 1e, inset). The high reaction yields can be attributed in large part to the combination of two factors: 1) close lattice matching between $NaYF_4$ and $NaLuF_4$ and 2) distinct separation between the nucleation and growth stages.[8] Indeed, our epitaxial-growth technique works well with hybrid $NaYF_4$, $NaYbF_4$, and $NaLuF_4$ systems, where internal stress or strain due to lattice mismatch is insignificant (Figure S6 in the Supporting Information).

The compositional difference of the core–shell structure was further revealed by elemental mapping (Figure 1f). It is important to note that a trace amount of Yb^{3+}/Tm^{3+} is particularly useful for optically characterizing the shell thickness and growth orientation. For example, elemental Yb and Lu in a $NaYbF_4$@$NaLuF_4$ crystal are hardly distinguishable by electron microscopy techniques owing to the similarity in their ionization energy (Yb-L_α = 7.4 keV and Lu-L_α = 7.6 keV) (Figure S7). In stark contrast, the dual-color emission of the microcrystals can be conveniently used to reveal the heterogeneous, core–shell crystal structure. Interestingly, the epitaxial growth orientation was found to be predominant along *a* axes rather than *c* axis, as evidenced by the difference between diameter (ca. 1.6 μm) and thickness (ca. 0.2 μm; Figure S8). The epitaxially grown shell layer can effectively prevent the surface quenching effect. As such, we observed a 30% enhancement in emission peak intensity for a single microparticle after surface passivation (Figure 1g).

To shed light on the growth mechanism and especially the growth kinetics of shell layers, we carried out five parallel experiments by reacting emissive $NaYF_4$:Yb/Er microcrystals with non-emissive $NaYbF_4$ shell precursor. The reactions were stopped at different times to yield information about the evolution of the crystal epitaxy (Figure S9). Notably, the gram-scale synthesis of highly uniform core–shell microcrystals was made possible by the bottom-up epitaxial growth strategy, thereby providing sufficient samples to enable appropriate statistical analysis. The comparison of luminescent micrographs obtained from different samples reveals that the epitaxial growth initiates from the seed and proceeds symmetrically along the sixfold crystal axis (Figure 2a, inset). Electron microscopic imaging of the samples obtained after 2 h reaction revealed a marked increase in the radial diameter of the microcrystals from 1.6 to 5.4 μm (Figure 2a and Figure S10). Importantly, our kinetic study makes possible to estimate the rate of epitaxial growth at different time intervals.

The epitaxial growth process of $NaYF_4$@$NaYbF_4$ core–shell crystals can be divided roughly into three stages: 1) nucleation of small oriented islands comprising shell precursor, 2) growth and coalescence of the nuclei into a continuous shell layer, and 3) Ostwald ripening to form large crystals. It is considered that the initial growth of the core–shell crystals results in a high density of cubic-phase $NaYbF_4$ nanoparticles. At an elevated temperature (ca. 220 °C), these nanoparticles start undergoing phase transition to form hexagonal-phase crystallites, which subsequently grow onto a seed crystal. On longer time scales, the primary core–shell crystals are expected to become stabilized against further growth if there is sufficient ligand (citric acid) passivation.

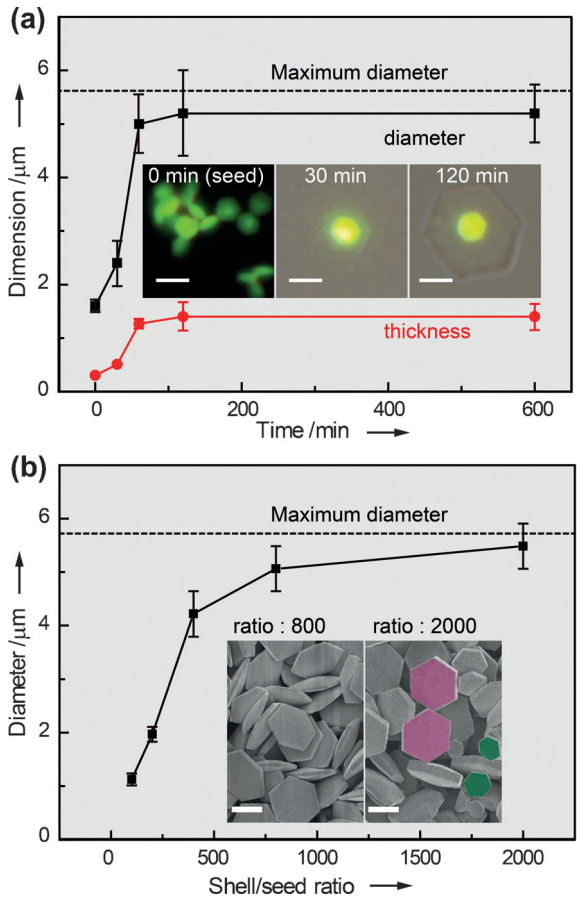

Figure 2. a) Size measurements of the core–shell $NaYbF_4$ crystals versus the reaction time for epitaxial growth. Note that green-emitting $NaYF_4$:Yb/Er (5/0.5 mol%) crystals (1.6 μm in diameter) were used as seeds. Inset: the corresponding optical micrographs of the products obtained at different times. b) Diameter measurements of the thermodynamic products versus the shell-precursor-to-seed feeding molar ratio. Inset: the corresponding SEM images of the core–shell $NaYbF_4$ crystals obtained at a shell/seed ratio of 800 and 2000, respectively. The phase separation (highlighted in pink and green colors) indicates that the crystal epitaxy is limited by a maximum size. Note that small $NaYbF_4$:Er (0.5 mol%, 150 nm in diameter) nanodisks were used as seeding crystals in the thermodynamic study. All scale bars are 2 μm. The error bar represents the standard deviation of the size measured for around 100 particles.

We further investigated the dependence of particle size on the shell precursor-to-seed molar ratio. It was found that the mean diameter of the $NaYbF_4$:Er@$NaYbF_4$ crystals increased from 1.1 to 4.2 μm with increasing shell precursor-to-seed ratios from 100 to 800 (Figure 2b and Figure S11). Such findings enable a versatile method to produce upconversion particles with tunable diameters over a large domain. The largest particles of approximately 5.4 μm in diameter were formed with a shell precursor-to-seed ratio of 2000 (Figure 2b). Because of phase separation, the particle size cannot be further increased by increasing shell precursor-to-seed ratio. Without the seed crystals, the $NaYbF_4$ shell precursor grows, under identical experimental conditions, into uniform crystals with a feature size of around 5.7 μm (Figures S12 and S13). The maximum size is likely limited by the dynamic balance between surface crystallization and dissolution under hydrothermal conditions.[7d]

To control the orientation of epitaxial growth, we developed a hydrothermal procedure that afforded rod-like $NaYbF_4$ crystals (Figure S5). During the synthesis, ethylenediaminetetraacetic acid (EDTA), instead of citric acid, was used as surfactant to regulate an orientated growth along the *c* axis.[7b,9] Importantly, the epitaxial growth preference along the *c* axis is maintained even in the presence of seeds, allowing segmented crystals to be generated as shown in Figure 3a. It is worth noting that the size of epitaxially grown components increases with increasing epitaxy precursor/seed ratio (Figure 3b–d, Figure S14), a trend which is similar to that observed in synthesizing plate-like crystals. To probe the

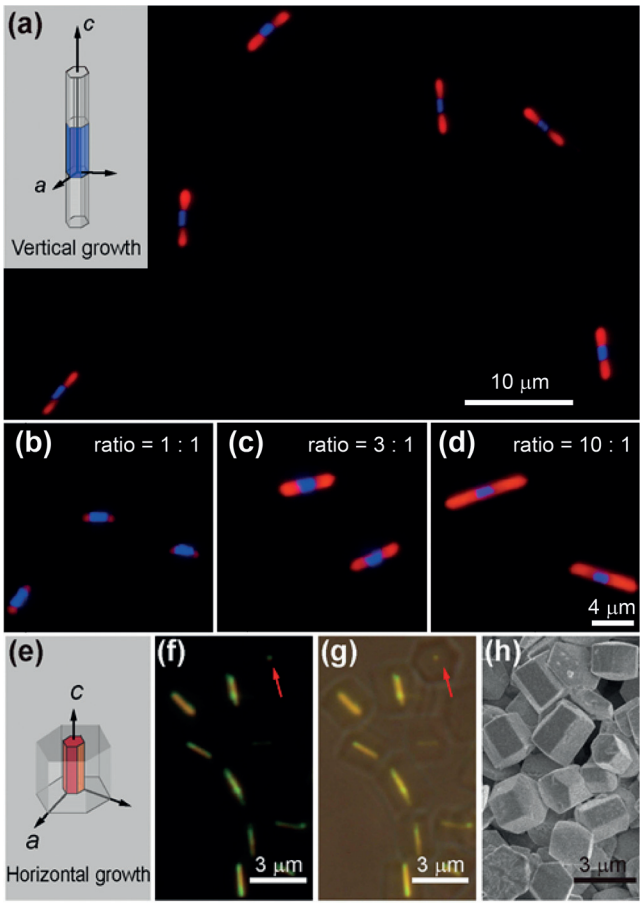

Figure 3. Epitaxial orientation control over *c* and *a* axes by using rod-like $NaYF_4$ crystals as seeds. a) An optical micrograph showing the dual-color emission of segmented one-dimensional crystals comprising $NaYbF_4$:Er(0.5 mol%)/$NaYF_4$:Yb/Tm(5/0.5 mol%)/$NaYbF_4$:Er(0.5 mol%). Insert: schematic representation of the vertical epitaxial growth of the seed. b–d) Luminescent micrographs of segmented crystals with varied lengths. The length can be precisely controlled by adjusting the shell precursor-to-seed ratio in the reaction system. e) Schematic representation of horizontal epitaxial growth. f,g) Optical micrographs of the as-synthesized core–shell hexagonal disks comprising $NaYF_4$:Yb/Er(20/0.5 mol%)@$NaYbF_4$. The red arrows highlight a typical hexagonal cross-section of the core/shell disks. h) Scanning electron microscopic image of the core–shell disks. Note that all luminescent images were taken under laser excitation at 980 nm.

effect of seeding crystal morphology on epitaxial growth, we used rod-shaped crystals as seeds to carry out epitaxial growth of crystals under the same conditions as described for producing $NaYbF_4$ microdisks. Surprisingly, we found that the crystals grow much faster along the *a* axes than *c* axis, resulting in plate-like crystals with a well-defined hexagonal structure (Figure 3 e–h). This clearly suggests that the effect of experimental conditions on epitaxial growth orientation is much stronger than does the shape of seeding crystals (Figure S15).

On the basis of the above experiments, a fundamental principle underlying epitaxial growth can be generalized, that is, the growth orientation of $NaLnF_4$ crystals is not determined by the morphology of seeding crystals. Instead, the choice of the surfactant (EDTA or citric acid) plays an indispensable role in controlling epitaxial orientation. The large binding affinity of EDTA molecules on (100) crystal facet relative to (001) facet promotes the anisotropic growth of the crystals along *c* axis.[7] In contrast, the use of citric acid molecules favors the crystals' growth along *a* axes because of selective molecular binding on the (001) crystal facet. Significantly, such growth habits can be harnessed to create multicolor upconversion crystals at the single-particle level. To validate this hypothesis, we successfully synthesized tri-colored microrods by stepwise feeding $NaYF_4$:Yb/Tm seeding crystals with precursors of different doping combinations (Yb^{3+}/Tm^{3+} or Yb^{3+}/Er^{3+}), as shown in Figure 4 a–c. Following a similar multi-step procedure, hexagonal-shaped, tri-colored microplates can also be synthesized (Figure 4 d–f). It should be noted that the product yields tend to decrease with increasing levels of complexity in emitting color combinations.

In conclusion, we developed a hydrothermal-based epitaxial growth technique for controlled synthesis of hybrid upconversion microcrystals that are able to emit multicolor at single-particle levels on near-infrared light excitation. The ability to create multicolor barcodes on a single particle may provide new platform for fundamental investigations of energy transfer between lanthanide dopants at the nanoscale. The ready accessibility of these optical barcodes in large scale is also likely to enable anti-counterfeiting and multiplexing labeling applications.

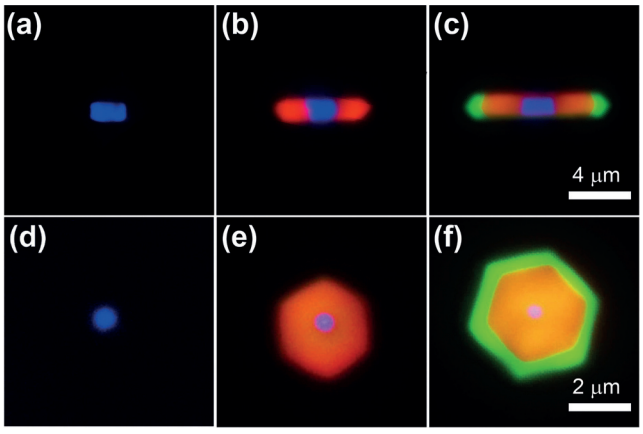

Figure 4. a–c) Optical micrographs showing the evolution of a rod-like crystal at different stages. a) $NaYF_4$:Yb/Tm (60/2 mol%) microrod used as the seed. b) tri-blocked microrod with the red segment composed of $NaYbF_4$:Er (2 mol%). c) tri-colored microrod with the green segment made of $NaLuF_4$:Yb/Er (5/2 mol%). d–f) Optical micrographs showing the evolution of a plate-like crystal. The precursor compositions for epitaxial growth are identical to those used for microrod synthesis. Note that all photoluminescent images were taken under excitation with a 980-nm laser.

Acknowledgements

The work was supported by the Singapore Ministry of Education, the National Natural Science Foundation of China (grant no. 21471109 and 21371095), and the Natural Science Foundation of Jiangsu Province (No.: BK20130923).

Keywords: color multiplexing · core–shell structures · epitaxial growth · single crystals · upconversion

How to cite: *Angew. Chem. Int. Ed.* **2016**, *55*, 5718–5722
Angew. Chem. **2016**, *128*, 5812–5816

[1] a) B. Dabbousi, J. Rodriguez-Viejo, F. V. Mikulec, J. Heine, H. Mattoussi, R. Ober, K. Jensen, M. Bawendi, *J. Phys. Chem. B* **1997**, *101*, 9463–9475; b) J. Wang, J. Neaton, H. Zheng, V. Nagarajan, S. Ogale, B. Liu, D. Viehland, V. Vaithyanathan, D. Schlom, U. Waghmare, *Science* **2003**, *299*, 1719–1722.

[2] a) F. Wang, J. Wang, X. Liu, *Angew. Chem. Int. Ed.* **2010**, *49*, 7456–7460; *Angew. Chem.* **2010**, *122*, 7618–7622; b) F. Zhang, R. Che, X. Li, C. Yao, J. Yang, D. Shen, P. Hu, W. Li, D. Zhao, *Nano Lett.* **2012**, *12*, 2852–2858; c) P. Huang, W. Zheng, S. Zhou, D. Tu, Z. Chen, H. Zhu, R. Li, E. Ma, M. Huang, X. Chen, *Angew. Chem. Int. Ed.* **2014**, *53*, 1252–1257; *Angew. Chem.* **2014**, *126*, 1276–1281; d) J. Hao, Y. Zhang, X. Wei, *Angew. Chem. Int. Ed.* **2011**, *50*, 6876–6880; *Angew. Chem.* **2011**, *123*, 7008–7012; e) H. H. Gorris, O. S. Wolfbeis, *Angew. Chem. Int. Ed.* **2013**, *52*, 3584–3600; *Angew. Chem.* **2013**, *125*, 3668–3686; f) Q. Liu, Y. Sun, T. Yang, W. Feng, C. Li, F. Li, *J. Am. Chem. Soc.* **2011**, *133*, 17122–17125; g) Z. Li, S. Lv, Y. Wang, S. Chen, Z. Liu, *J. Am. Chem. Soc.* **2015**, *137*, 3421–3427; h) Y. Xiao, L. Zeng, T. Xia, Z. Wu, Z. Liu, *Angew. Chem. Int. Ed.* **2015**, *54*, 5323–5327; *Angew. Chem.* **2015**, *127*, 5413–5417; i) B. Voss, M. Haase, *ACS Nano* **2013**, *7*, 11242–11254.

[3] a) M. Haase, H. Schäfer, *Angew. Chem. Int. Ed.* **2011**, *50*, 5808–5829; *Angew. Chem.* **2011**, *123*, 5928–5950; b) F. Wang, R. Deng, J. Wang, Q. Wang, Y. Han, H. Zhu, X. Chen, X. Liu, *Nat. Mater.* **2011**, *10*, 968–973; c) G. Chen, H. Qiu, P. N. Prasad, X. Chen, *Chem. Rev.* **2014**, *114*, 5161–5214; d) S. Zeng, Z. Yi, W. Lu, C. Qian, H. Wang, L. Rao, T. Zeng, H. Liu, H. Liu, B. Fei, J. Hao, *Adv. Funct. Mater.* **2014**, *24*, 4051–4059; e) D. Yang, P. Ma, Z. Hou, Z. Cheng, C. Li, J. Lin, *Chem. Soc. Rev.* **2015**, *44*, 1416–1448; f) Y. Sun, W. Feng, P. Yang, C. Huang, F. Li, *Chem. Soc. Rev.* **2015**, *44*, 1509–1525; g) H. Schäfer, C. Hess, H. Tobergte, A. Volf, S. Ichilmann, H. Eickmeier, B. Voss, N. Kashaev, J. Nordmann, W. Akram, B. H. -Azanza, M. Steinhart, *Small* **2015**, *11*, 931–935; h) Y. Min, J. Li, F. Liu, E. K. L. Yeow, B. Xing, *Angew. Chem. Int. Ed.* **2014**, *53*, 1012–1016; *Angew. Chem.* **2014**, *126*, 1030–1034; i) K. Zheng, Z. Liu, C. Lv, W. Qin, *J. Mater. Chem. C* **2013**, *1*, 5502–5507; j) J. Lai, Y. Zhang, N. Pasquale, K. Lee, *Angew. Chem. Int. Ed.* **2014**, *53*, 14419–14423; *Angew. Chem.* **2014**, *126*, 14647–14651; k) R. Martin-Rodriguez, R. Valiente, F. Rodriguez, F. Piccinelli, A. Speghini, M. Bettinelli, *Phys. Rev. B* **2010**, *82*, 075117; l) S. Nam, Y. Bae, Y. Park, J. Kim, H. Kim, J. Choi, K. Lee, T. Hyeon, Y. Suh, *Angew. Chem. Int. Ed.* **2011**, *50*, 6093–6097;

Angew. Chem. **2011**, *123*, 6217 – 6221; m) X. Chen, D. Peng, Q. Ju, F. Wang, *Chem. Soc. Rev.* **2015**, *44*, 1318 – 1330; n) X. Ye, Y. Liu, Y. Lv, G. Liu, X. Zheng, Q. Han, K. A. Jackson, X. Tao, *Angew. Chem. Int. Ed.* **2015**, *54*, 7976 – 7980; *Angew. Chem.* **2015**, *127*, 8087 – 8091.

[4] a) B. Zhou, B. Shi, D. Jin, X. Liu, *Nat. Nanotechnol.* **2015**, *10*, 924 – 936; b) M. Bettinelli, L. Carlos, X. Liu, *Phys. Today* **2015**, *68*, 38 – 44; c) N. J. J. Johnson, A. Korinek, C. Dong, F. C. J. M. van Veggel, *J. Am. Chem. Soc.* **2012**, *134*, 11068 – 11071; d) H. Schäfer, P. Ptacek, O. Zerzouf, M. Haase, *Adv. Funct. Mater.* **2008**, *18*, 2913 – 2918; e) J.-C. Boyer, F. Vetrone, L. A. Cuccia, J. A. Capobianco, *J. Am. Chem. Soc.* **2006**, *128*, 7444 – 7445.

[5] a) M. J. Dejneka, A. Streltsov, S. Pal, A. G. Frutos, C. L. Powell, K. Yost, P. K. Yuen, U. Müller, J. Lahiri, *Proc. Natl. Acad. Sci. USA* **2003**, *100*, 389 – 393; b) Z. Jacob, L. V. Alekseyev, E. Narimanov, *Opt. Express* **2006**, *14*, 8247 – 8256.

[6] a) C. Zhang, J. Y. Lee, *ACS Nano* **2013**, *7*, 4393 – 4402; b) Y. Zhang, L. Zhang, R. Deng, J. Tian, Y. Zong, D. Jin, X. Liu, *J. Am. Chem. Soc.* **2014**, *136*, 4893 – 4896.

[7] a) X. Wang, J. Zhuang, Q. Peng, Y. Li, *Inorg. Chem.* **2006**, *45*, 6661 – 6665; b) C. Li, Z. Quan, P. Yang, J. Yang, H. Lian, J. Lin, *J. Mater. Chem.* **2008**, *18*, 1353 – 1361; c) F. Zhang, Y. Wan, T. Yu, F. Zhang, Y. Shi, S. Xie, Y. Li, L. Xu, B. Tu, D. Zhao, *Angew. Chem. Int. Ed.* **2007**, *46*, 7976 – 7979; *Angew. Chem.* **2007**, *119*, 8122 – 8125; d) W. Beckmann, *Crystallization: Basic Concepts and Industrial Applications*, 1st ed., Wiley, Hoboken, **2013**.

[8] a) N. T. Thanh, N. Maclean, S. Mahiddine, *Chem. Rev.* **2014**, *114*, 7610 – 7630; b) J. Park, E. Lee, N. M. Hwang, M. Kang, S. C. Kim, Y. Hwang, J. G. Park, H. J. Noh, J. Y. Kim, J. H. Park, *Angew. Chem. Int. Ed.* **2005**, *44*, 2872 – 2877; *Angew. Chem.* **2005**, *117*, 2932 – 2937.

[9] a) J. H. Zeng, J. Su, Z. H. Li, R. X. Yan, Y. D. Li, *Adv. Mater.* **2005**, *17*, 2119 – 2123; b) H. Qiu, G. Chen, L. Sun, S. Hao, G. Han, C. Yang, *J. Mater. Chem.* **2011**, *21*, 17202 – 17208.

Received: December 15, 2015
Revised: February 4, 2016
Published online: April 1, 2016

